

# Development of a Miniature InGaAs Spectral Analyzer

Quiesup Kim

Jet Propulsion Laboratory, California Institute of Technology  
Pasadena, California 91109, U. S. A.

## 1. Introduction

Reflectance spectroscopy provides a means for mapping surface mineralogies rapidly. As an example, a reflectance absorption spectrum of a mixture of common rock forming minerals is shown below. Each mineral is a different molecule that absorbs energy in a region of the whole excited spectrum. From the spectrum the minerals can be identified and with radiative transfer analysis the relative concentrations of the minerals can be determined as shown in **Figure 1**.

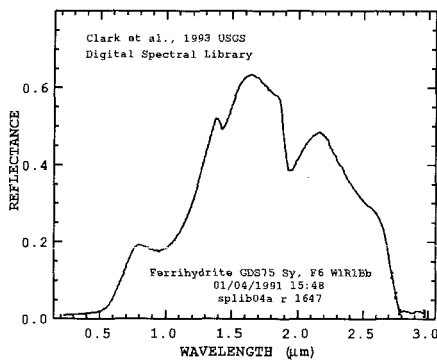


**Figure 1. Typical surface absorption spectrum of the Ferrihydrite.**

Terrestrial materials have long served as analogs of the Martian surface, both chemically and spectrally. For example, AVIRIS has sampled areas of California, Nevada, and Utah, having surface mineralogy that includes numerous clays, sulfates, iron oxides, carbonates and other minerals. The average terrestrial spectrum shows overall spectral shape and albedo level to similar spectra of Martian bright regions. Some areas containing hematite have visible spectrum that is very similar to the spectrum of Mars. The terrestrial spectra show strong clay absorption at 2.2 microns (OH). The strength of comparable features (at 2.2 microns) in spectra of Mars are about a factor of 50 less, implying very low global abundance of OH-bearing materials with 2.2-microns absorptions. This implies a weathering history on Mars that differs substantially from that for Earth.

"Several terrestrial minerals have been proposed as spectral analogs for Martian surface materials, and two groups in particular, the palagonites and the montmorillonites, have proven exceptionally popular. However, neither provides a perfect match to the observations, and the diagnostic 2.2-microns cat ion-OH vibrational absorption exhibited by most terrestrial clays has yet to be detected in spectra of the Martian surface. Mixtures of 5.0, 3.0, 1.0, and 0.5 weight % montmorillonite (SAZ-1) in a spectrally bland basaltic powder having a 2.2-microns albedo similar to that of Mars have been measured. The **Figure 2** shows the variation of band depth with clay content in the mixtures. For mixtures of as little as 5.0 weight % of clay, the 2.2-microns band is readily separated from the continuum, and is clearly distinguishable down to 1.0 weight %. Below 0.5 weight %, however, **existing technology cannot achieve sufficient signal-to-noise** to separate the 2.2-microns absorption from background. Between 5 to 0.5 weight % clay, band depths ranged from 0.013 to 0.0011 for the basalt-montmorillonite mixtures. Examination of the literature reveals that the upper limit to the 2.2-microns band depth for Martian spectra is 0.0007 micron 0.0010 (Clark, 1992, Reference 1), easily less than that for the 0.5 weight % clay mixture used in this study. This would imply that Martian soils of as much as 1 weight % clay could be ruled out on the basis of available spectroscopic data."<sup>2</sup>

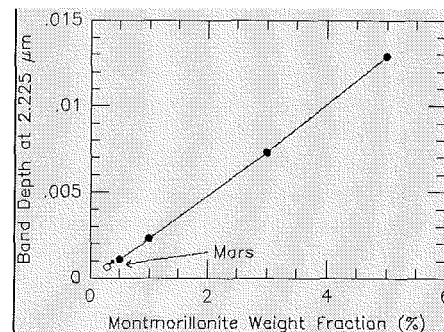


**Figure 2. Clay absorption feature depth as a function of abundance (Reference 2).**

The amount of clay minerals on the surface of Mars is much lower than expected, less than two percent of that found on earth. These low values may provide another clue to deciphering the mystery concerning the evolution of the surface and the potential for prior life on Mars. Clays may be important to the formation of life, perhaps as surfaces to which large molecules could stick. If clays never formed in abundance on Mars, life may not have been able to develop. If some processes are destroying clays, then those processes might also have been hostile to the formation of life.

For decades scientists have debated the mineral composition of the Martian surface. Its red color was assumed to be caused by the presence of weathered iron oxides--also known as rust. (Refer **Figure 1**) Since iron oxides and clay are common products of the weathering process on Earth, they were assumed to be equally common on Mars. None of the spacecraft that have landed on Mars so far have been able to directly determine what minerals are present on Mars – though APX experiments have provided partial measurements of the underlying composition.

Mapping mineralogy is important to establishing the sequence of events, which formed the present Martian surface. Particularly important is the identification of rocks and minerals formed in the presence of water since water appears to have played a dominant role in shaping the topography of Mars and is considered to be one of the key ingredients for formation of life. Current and past Mars missions have already sent back views of the Martian surface that seem to show evidence of dry riverbeds, flood plains, rare gullies on Martian cliffs and crater walls, and sedimentary deposits that suggest the presence of water at some point in the history of Mars.

The current body of evidence for these structures arises largely from interpretations of albedo (and scattering) differences mapped in the visible. These differences can be much more evident and/or diagnostic when observed at other wavelengths that should produce higher albedo contrasts corresponding to different mineralogic regimes. In particular, in the near-IR region, the degree of oxidation of basalts affects the slope from 0.5 to 0.8 microns, iron oxides (Fe 3<sup>+</sup>, Hematite, Goethite) have diagnostic bands between 0.5 and 1 micron, the "ferrous" band at 0.9-1.1 microns and around 1.5 microns can discriminate between various pyroxenes and olivines, and the 2-2.5 micron region can be used to differentiate between various clays, water of hydration, and similar OH-bearing materials.

The albedo contrasts can be (and for Mars, frequently are) masked by desert varnish, dust coating and atmospheric scattering, all of which tend to subdue or even mask underlying spectral features. These problems can be ameliorated by finding or creating fresh surfaces (requires high resolution or close proximity) and/or by having very good signal-to-noise to allow discrimination of absorptions having low contrast. The latter approach is also enhanced by utilizing high spatial resolution (to get limited mineralogic variation in a single field) and high illuminance.

The InGaAs array, and the high throughput of the convex grating is ideally suited to address the challenges discussed above. The spectral range of the detector provides excellent crossover coverage between the silicon (e.g. CCD) devices used for imaging and the microthermopile devices used for longer wavelengths. Its high D\* (>10<sup>12</sup> cm-Hz<sup>1/2</sup>/W at 200K - **Figure 3**)<sup>3</sup> at 1 micron is ideally suited for utilizing the very diagnostic "ferrous" bands and for detecting very small (or subdued) spectral variance(s). The combination of high D\* and appropriate spectral range also make the device ideally suited for (near-field) Raman spectroscopic observations. The modest cooling requirements make it usable on the Martian surface (utilizing either thermal electric or night time "thermal mass" cooling). The aerial array allows elimination of a grating scanning mechanism and enables 1 dimensional spatial extent, summation to improve signal to noise, or time domain spectroscopy, depending on the application. In addition, the relatively high speed (>3.5x10<sup>7</sup> pixels/s) provided by the APS readout can lead to relaxed pointing stability requirements, ease integration with other instruments, and make feasible novel surface chemistry experiments such as monitoring laser ablation of surface coatings or measuring fluorescence decay.

## 2. Objectives

The objective of this study is to develop a prototype spectrometer subsystem suited for mapping mineral differences on Mars surface from a lander or rover platform. This prototype will be implemented utilizing an InGaAs 2D focal plane array, monolithically integrated with an InP JFET amplifier and readout multiplexer, and an optics train utilizing a micromachined convex diffraction Grating for the distortion-free dispersive optical element.

### 2.1 Specific Aims

There is a crossover point between the contributions

of reflected and emitted radiation that depends on the solar spectrum and surface temperature. For Mars, this (minimum) occurs at about 2.6 microns. For the design of surface spectral instruments that is a natural place to transition from band-gap to bolometer (etc) type detectors, thus avoiding the high-power cooling requirements for band-gap devices used at longer wavelengths. Until now, it was also necessary to use different detectors at a boundary located at 1 micron because of the responsivity of silicon and (for instance) lead sulfide detectors. The location of this transition region is unfortunate, because the low responsivity makes it difficult to utilize this very diagnostic spectral region.

### 3. Detector description

The InGaAs array spans the gap that represents the end (~0.9 microns) of silicon sensitivity and the start (~1 micron) of InSb (See **Table I**), lead salts, and HgCdTe detectors. **The monolithic sensor eliminates the need for hybridization with a silicon multiplexer, and also allows the sensor to be front illuminated, making it sensitive to visible as well as IR radiation.**<sup>4,5</sup> This provides the opportunity to utilize a single focal plane array (or focal plane type, depending on implementation for imaging and spectroscopy, and to relate spatially visible albedo ("color and shading") to IR albedo ("Composition, temperature, and structure"). The high  $D^*$  of this array also permits use in low-light level applications (Raman spectroscopy, time-resolved spectroscopy, and scattering by dust and aerosols) - which makes the technology particularly interesting for packages to be landed on Mars. (Refer **Table II**)

**Table I. Comparison of Detector Operations**

	<b>MISA</b>	<b>AVIRIS</b>
Detector Material	InGaAs	Si/InSb
Detector Configuration	Monolithic	Hybrid
FPA	2D(64x64) APS	1D(614)
Spectral Ranges (μm)	VIS/NIR (0.5-2.5)	VIS/NIR (0.3-0.9/3.0-6.0)
Operating Temperature	-65°C	-196°C
Cooling	TEC	LN <sub>2</sub>

**Table II. Modes of Operation**

<b>InGaAs Application</b>	<b>Comment</b>
Camera	Filters (Interference, Liquid crystal)
Spectrometer	Filters or grating
Time-resolved spectroscopy	Nanosecond on up
Raman Spectroscopy	Measure forbidden transitions
Scattering	Can measure size dependence

For this proposal, we have chosen to implement and test the three spectrometer applications, because these three would have high utility for the planetary program, do not have alternative instruments available, and provide the most demanding use of detector sensitivity.

State-of-the art focal plane array technology for imaging in space utilizes charge-coupled devices (CCDs) which are made of silicon semiconductor materials for the visible range, and cryogenically cooled linear arrays of InSb or HgCdTe - some bonded to CCDs/complementary meta-oxide semiconductor (CMOS) for readout, for infrared. These have all the advantages in signal detection and processing of previous point detection systems. However, CCDs have problems in long-term stability, sensitivity, and fast dynamic information transfer due to the required high charge transfer efficiency (>99.93%) for these devices. High power consumption, cooling requirements, and limited wavelength ranges are the main obstacles that must be overcome in order to construct miniaturized, mobile, integrated, smart, and multifunctional imagers in one chip for potential use in landed missions and missions with severe resource limitations.

State-of-the-art InGaAs near-infrared (NIR) focal plane arrays (FPA) are now available. The current generation of square format InGaAs FPAs gives expected improved performance. This FPA has a higher density of pixels than any other single material currently available in the range of 0.5 – 2.5 μm band at near room temperature as shown in **Table III**. The FPAs are made of In<sub>x</sub>Ga<sub>1-x</sub>As by mixing InAs to GaAs and stacking the materials from x = 0.53 to 0.82 to increase the responsivity of the multi-layered quantum well structures. They are responsive over the spectral range (0.5 – 2.5μm) of visible and near IR.<sup>4,5</sup> The resultant InGaAs FPA has superior detectivity in the range of 0.5 – 2.5 μm compared with other detectors, especially near room temperature.<sup>6-8</sup> (**Figures 3 and 4**) This MISA subsystem will use the InGaAs sensor array

monolithically integrated with InP JFETs for readout control and signal amplification for front signal illumination.

**Table III. Characteristics of an available InGaAs Focal Plane Array**

---

Material: $\text{In}_x\text{Ga}_{1-x}\text{As}$ substrate $x = .82$
Material thickness: 5-18 $\mu\text{m}$ thick
Format: 64 x 64
Pixel Size: 150 $\mu\text{m}$ x 150 $\mu\text{m}$
Spectral Bandwidth: 0.5 $\mu\text{m}$ to 2.5 $\mu\text{m}$
Peak Detectivity: $10^{12}$ $\text{cm Hz}^{1/2}/\text{W}$ at a temperature of 200K
Quantum efficiency: 65 % at 2.0 $\mu\text{m}$
Estimated power consumption: <130mW

---

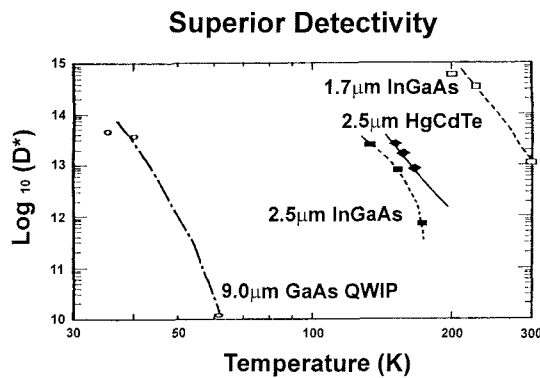


**Figure 3. Comparison of detectivity among the most popular infrared detectors. InGaAs exhibits superior detectivity, permitting detection of small spectral variances.**

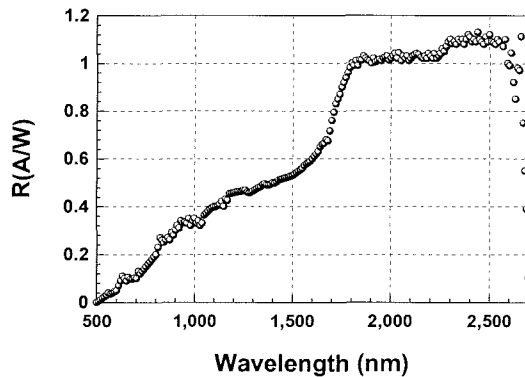


**Figure 4. Spectral Response of the InGaAs detector. The detector is responsive to the VIS and NIR over the range of 0.5 ~ 2.5  $\mu\text{m}$ .**

### 3.2 Optical Train

The distortion-free dispersing capability of the grating required for spectral imaging applications is limited to a spectral range with a minimum to maximum ratio of 1:2. The designed convex grating will combine three different regions of concentric gratings to cover the whole optical range (0.5 – 2.5  $\mu\text{m}$ )

**A). State-of-the-art InGaAs near-infrared (NIR) focal plane arrays (FPA)** will be used and its responsivity will be characterized. The current generation of a front-illuminated rectangular format InGaAs FPA has a higher performance than anything currently available as a single detector in the VIS/ NIR band at near room temperature. The JPL-developed InGaAs FPA, monolithically integrated with InP JFETs, will be controlled by readout circuit boards for testing. The final selection will be made for the best detectivity ( $D^* > 1\text{E}10^{12}$   $\text{cm Hz}^{1/2}/\text{W}$ ) at 2.0  $\mu\text{m}$  on a 64 x 64 focal plane array with a pixel pitch of 150  $\mu\text{m}$ . (**Table III**)

Spectral resolution of the proposed subsystem will be determined by spreading the dispersed beam over all the columns (64) of the 2-D InGaAs FPA. Consequently, the frequency or wavelength of the light received by each pixel could be identified from the position of the pixel along its row (see **Figure 6a**). When a lens is used to image the target scene onto the FPA, the position of each pixel along a column provides a spatial resolution element for each spectrum.

**B). Spectral dispersion** will be achieved by utilizing a convex grating to be fabricated at JPL using the JPL technique described in the references.<sup>9-15</sup> The surface contour of the substrate is first mapped to regions within which the elevation changes by no more than one focal depth. The diffractive optical element pattern is then divided into sub-patterns corresponding to those regions. For the case of a spherical surface, the sub-patterns are annuli. Each sub-pattern is exposed in sequence, adjusting the focus, deflector calibration, and deflector rotation for each pattern. **Figure 6a** illustrates the general configuration of the convex grating with respect to the InGaAs FPA.

**C). Integrated Readout Circuit Boards (IRCBs)** will be fabricated to connect the FPA to the existing Microelectronic Advanced Laser Scanner (**MEALS**) laboratory test set. (**Figure 5**) Since the Multiplexer hybridized to the InGaAs FPA includes an auto zero integrator, background suppressor, and buffer

preamplifier, IRCB will be a pixel test personality card and a mother board to control the individual pixel I/O ports by shifting the digital connector using the system clock and power suppliers.

**D). Testing of the FPA, multiplexer, and optical train** will be characterized for throughput and noise at the component and system level. Tests for cross talk and spectral discrimination will be performed at the system level using triple spectrometer, reference spectral materials and a precision black body. The total system performance will be demonstrated with a mineral target, measuring a part of the pyroxene solid solution series.<sup>16</sup> The prototype will additionally be tested in Raman mode (which requires very high SNR) using one of the configurations of the MEALS test set at JPL, as shown in **Figure 5**.

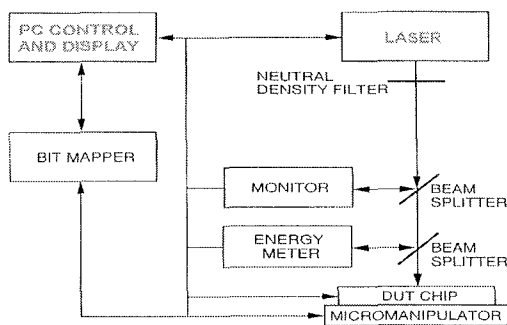


**Figure 5.** Block diagram of the test setup using the Microelectronic Advanced Laser Scanner (MEALS).

#### 4. Technical Approach

**Figure 6a** shows the MISA subsystem: a 2-D InGaAs FPA combined with a convex grating to test detector response and spectrometer throughput of these two key elements. The MISA subsystem will be tested by PC that controls the system clock of the Pulse Instruments (PIs) and the readout channels of the FPA. The laboratory test setup for the MISA system also includes a beam splitter that is mounted on a micromanipulator, a mechanical chopper and a filter. The implementation of MISA in this proposal uses various external broadband sources, external monochromatic sources, and an external single-frequency laser to actively excite a target.

The expected high  $D^*$  makes MISA suited to both passive imaging spectroscopy and (near-field) Raman applications (**Figure 6b**). The dispersed light from the grating will be detected by a row of the two-dimensional rectangular InGaAs focal plane

array (64x64). Consequently, the wavelength or frequency of the light received by each pixel can be identified from the position of the pixel along its row (64). Each column pixel represents a spatial position (in imaging mode) or can be sampled sequentially (and rapidly) for time-domain applications. The FPA will be operated in conjunction with APS readout control, 3-D readouts, and pixel-data-processing circuits.<sup>3, 17-18</sup> When tested in an absorption spectral configuration, light returning from the target will be reflected by a beam splitter prior to discrimination of the excitation light by a low frequency pass filter. Only the induced emitted light from the target will be introduced to the convex diffraction grating.

Light returning from the target, after filtering the excitation light, would be spectrally dispersed by the built-in grating prior to reaching the detector arrays in this case, along the columns of the zeroth row (P00, P01, P02, P03, ...) of an FPA array. Hence, by processing the readouts from the pixels in this row at the same time, one could obtain a wavelength-resolved characteristic spectrum of the target for its identification.

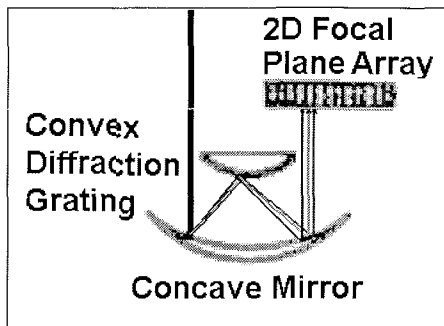


**Figure 6a.** Proposed MISA Subsystem: Magnified version of the gray area of the Figure 6b.

#### 5. Limitations

Due to the optoelectronic characteristics of the intended material for this proposed MISA, the spectral response would be limited to the wavelength range of 0.5 - 2.5  $\mu\text{m}$ . However, the concept of the instrument can be applied to any interested space mission by replacing the sensor material accordingly. The advantage of the monolithic InGaAs APS FPA is, though, that one is able to have the superior detectivity by front illumination for the visible and near infrared functional observation without the backside-thinning, indium bump bonding, and the bulky cryogenic cooling system that is required of most infrared detectors.

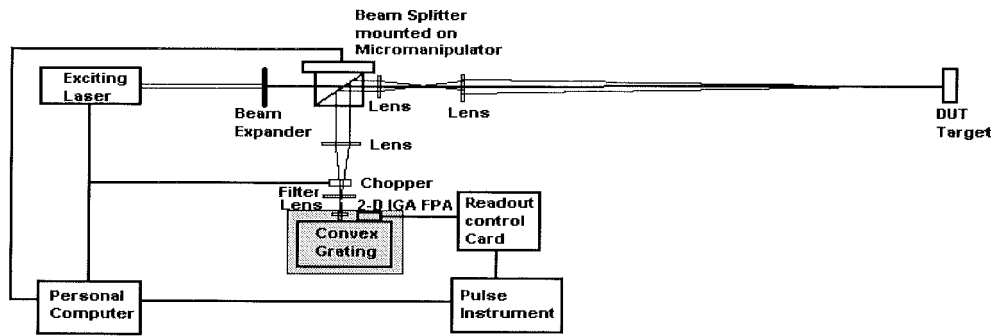


Figure 6b. Mars straw man configuration. The fore optics would have a near field component for Raman use and afar field capability for passive imaging spectroscopy. Gray area is the Subsystem (6a) described.

## 6. Anticipated Results

InGaAs detectors span a spectral range, 0.5 to 2.5  $\mu\text{m}$ , that is of great utility for planetary science (see Table IV). This particular wavelength span permits relating visible albedo variations to compositional regimes with the same detector. The spectral range includes the sulfur transition band (Io), ferric and ferrous iron (Earth, Mars, Galilean satellites, Asteroids),  $\text{CO}_2$  bands (Venus, Earth, Mars, Europa),  $\text{NO}_x$  bands (Titan),  $\text{H}_2\text{O}$  and hydration bands (Earth,

Mars, Europa).<sup>1, 19-31</sup> It is important to note that spectrometers in the visible range have not been included in prior deep space payloads (because the spectral range is accessible through Earth's atmospheric window), but are important for *in situ* (and high-spatial resolution orbital) payloads on Mars where the spatial resolution is very much better than that available from earth. In this situation, classification of the terrain by precise color would be much more productive than by utilizing a few filters in a camera.

Table IV. Planetary applications for InGaAs spectral range

Species	Planet	Comments
$\text{S}_x$	Io	
$\text{H}_2\text{O}$ , Hydration Products	Mars, Europa, Earth	
$\text{CO}_2$	Mars, Europa,	
$\text{NO}_x$	Titan	
$\text{Fe}^{3+}$	Earth, Mars, Europa, Moon Asteroids	
$\text{Fe}^{2+}$	Moon, Mars, Asteroids, Galilean satellites, Comets	Olivine, Opx-CPx, Plagioclase
Chlorophyll	Earth, Europa	
$\text{CH}_4$	Triton	
$\text{H}_2\text{SO}_4$	Venus	
Thermal measurements	Io, Earth	Lavas above $\sim 500\text{K}$

### 6.1 Perceived Impact of this Work

#### Straw man Rover configuration

It is intended that this prototype lead to a spectrometer suited for deployment on a Mars07 rover. The characteristics required for surface use include low power, mass and low volume. The high sensitivity and SNR expected from the prototype focal plane and grating combination proposed here

would be suited for combined standard reflectance spectroscopic and Raman spectroscopic operation. In an operational configuration this prototype would be combined with fore optics, a laser diode, and a beam splitter. The operational configuration would be used in standard reflectance mode for survey operations and in both standard reflectance and Raman mode for near-field examination of the mineralogy of rocks and grains. Preliminary estimates suggest that night

time cooling of a thermal mass combined with a thermal electric cooler mated to the focal plane would provide a net lowest power operation.

The proposed research will produce a bench-top instrument that can be demonstrated by thoroughly evaluating the performance of this new InGaAs focal plane array and readout multiplexer, and the system throughput and image quality of the detector/convex grating combination.

These evaluations will be performed utilizing the bench-top prototype. The parameters derived will be used to design a complete prototype instrument suited for use on the Martian surface.

The results derived from this research will provide an enabling technology for remotely determining the mineralogy of Mars surface material.

The InGaAs FPA is an unsealed focal plane array mounted in a 28-pin package. This configuration allows the user to modify the conditions for testing. The user can change the bias, gain, clocking rate, integration time, and temperature in Jet Propulsion Laboratory's focal plane array test setup. This provides a larger range of testing conditions. This focal plane array has similar specifications as the device in the dewar cooled camera plus the versatility of being able to operate under the user's conditions, i.e. variable temperature, larger reverse bias, etc. The following are the features of this array:

- 64x64 pixels on a 150  $\mu\text{m}$  pitch (9.6x9.6mm<sup>2</sup>)
- Uniformity 98%
- Sensitivity from 0.6 ~ 2.55  $\mu\text{m}$
- $D^* > 2.8 \times 10^{10}$  cm Hz<sup>1/2</sup>/W @1.55  $\mu\text{m}$  at 208K
- Full well capacity 1E7 photons
- Dark Current 100 nA
- Rise Time 0.041  $\mu\text{s}$

The room temperature InGaAs photodiode detector module is a photovoltaic type detector with a responsivity of 0.65 to 2.65  $\mu\text{m}$ . Compared to the un-cooled type Ge photodiode, the InGaAs photodiode has superior features such as smaller junction capacitance and larger shunt resistance. The InGaAs photodiode detector module has excellent performance at room temperature in the near IR to 2.65 $\mu\text{m}$ .

The detector assembly consists of an InGaAs photodiode mounted in a compact housing, which can be screwed directly on the slit of the MISA.

### **Spectral Response**

The spectral response of the thinned InGaAs diode array is from 0.50 nm to 2500 nm. The maximum sensitivity wavelength is located around 2400 nm and corresponds to 39% quantum efficiency.

### **Spectral Resolution**

A rectangular array provides broad wavelength coverage or high resolution but not both. The spectral resolution of this proposed subsystem is determined by both the total spectral coverage and the number of pixels in a row. Thus the spectral resolution of the proposed subsystem will be depend upon the total size of the subsystem housing.

### **Noise**

The noise components of an APS are shot noise, dark signal and read-out noise. APSs can be cooled thermoelectrically to reduce the dark signal and it's associated random noise.

### **Dynamic Range**

Potential well capacity is another important characteristic of the FPA. It is the measure of how much charge can be stored in an individual pixel. A chip with a larger full well capacity can record a higher signal level before saturating. This specification varies, depending on the **doping** of the InGaAs, architecture and **pixel size**. The quantum well capacity for this array is usually around 1E7 electrons. Well capacity and read out noise determine the dynamic range of the chip. The greater the well, the greater the dynamic range. In an APS, the most intense signal, the saturation level, is the potential well capacity and the weakest signal is limited by the read out noise. **MISA** will be equipped with a variable gain. This is extremely important in applications where we typically have very weak signals. By increasing the gain to measure signal levels which are very close to the noise, we can improve our signal to noise ratio while maintaining the same integration time. Or, we can achieve the same signal to noise ratio in less time. It is also useful for measuring more intense signal levels and enables you to take full advantage of the saturation limit of the APS.

### **Rapid Acquisition of Multiple Spectra**

The rectangular format permits near-simultaneous acquisition of 64 spectra, providing opportunity for push broom imaging and/or pixel summation for improved SNR.

## **7. Conclusion**

A highly sensitive, low noise, miniaturized VIS

/NIR imaging spectrometer subsystem based on a new, advanced InGaAs focal plane array and a new technology, micro-machined, high-throughput, distortion-free convex diffraction grating is presented. The goal of this paper is to define and develop a prototype non-cryogenic spectral analyzing instrument that fits within resource limits typical for a Mars Rover and that covers the wavelength region critical for understanding Mars surface chemistry.

The key improvements for this prototype over existing VIS/NIR systems is the ability to measure the full spectral range (0.5 to 2.5 microns) with a single, 2-dimensional detector array and a fixed grating without the need for cooling. This simplifies and reduces the scale of instrumentation that has historically been difficult to implement on planetary missions.

The two-dimensional InGaAs focal plane array used with this instrument is different from existing detector technology and permits a unique implementation with superior detectivity ( $D^*$ ) requiring no cryogenic cooling over a spectral range that is not spanned by any other single detector material. The high  $D^*$  of the array enables measurement of narrow bandwidths at low illumination levels, analysis of subtle absorption in spectra of mixtures, and high-speed measurement of reaction kinetics. The 2-D array permits mapping the image with a fixed grating, eliminating the spectral distortion created with grating motion. It can detect the characteristic visible/infrared optical signals of compositions (and isotopes) of interest for use in scientific investigations on future planetary missions {e.g. Fe [3+, 2+](olivine, pyroxene) (Mars, Io),  $\text{NO}_x$  (Titan),  $\text{H}_2\text{O}$  (Ice), salt hydrates, clays (Mars, Europa),  $\text{CO}_2$  (Mars)}. The micromachined convex grating, with sharper ruling edges, more precise blaze angles, and fewer required reflecting surfaces provides higher throughput and better image quality than that available from conventional replicated or ruled gratings.

The **MISA subsystem** will include: 1) integrating the InGaAs 2D focal plane array (FPA) on a miniature thermoelectrical cooler ( $-65^\circ\text{C}$ ) with sampling circuits without the cryogenic cooling system, 2) integration with JPL-developed miniaturized convex gratings, and 3) integration of a bench top instrument control system to demonstrate characteristic **mineral olivine** spectrum. The laser excited emission spectrometer then can be stimulated with a built-in advanced laser scanning (MEALS) system for an mobile object identification or target imaging applications.

## Acknowledgments

The research described in this paper was carried out by the Center for Space Microelectronics Technology, Jet Propulsion Laboratory, California Institute of Technology, under a contract with the National Aeronautics and Space Administration. Reference herein to any specific commercial product, process, or service by trade name, trademark, manufacturer, or otherwise, does not constitute or imply endorsement by the United States Government or the Jet Propulsion Laboratory, California Institute of Technology.

## References

1. Roger N. Clark, K. Eric Livo and Raymond F. Kokaly, Geometric Correction of AVIRIS Imagery Using On-Board Navigation and Engineering Data by U. S. Geological Survey, Summaries of 7<sup>th</sup> Annual JPL Airborne Earth Science Workshop, Jan 12-14, 1998.
2. American Astronomical Society, Division of Planetary Science, October, 1995 meeting in Hawaii.
3. Q. Kim, T. J. Cunningham, and E. R. Fossum, "Monolithic InGaAs JFET Active Pixel Image Sensor (MAPTIS)," Invited Paper, Proc. SPIE on Optoelectronic Integrated Circuits, Vol. 3006, p. 176, 1997, G. Olsen, "InGaAs fills the near-IR detector-array vacuum", Laser Focus World, Vol. 27(3), p. 21 (1991).
4. S. K. Mendis, S. E. Kemeny, R. C. Gee, B. Pain, Q. Kim, and E. R. Fossum, "Progress in CMOS Active Pixel Image Sensors", Proceedings of the SPIE on Charge-Coupled Devices and Solid State Optical Sensors IV, Vol. 2172, 1994
5. E. R. Fossum, "Active Pixel Sensors: Are CCD's Dinosaurs?", Proceed. of SPIE on Charge-Coupled Devices and Solid-State Optical Sensors III, Vol. 1900, 1993
6. Q. Kim, T. J. Cunningham, and E. R. Fossum, "Monolithic InGaAs JFET Active Pixel Image Sensor (MAPTIS)", Invited Paper, Proc. SPIE on Optoelectronic Integrated Circuits, Vol. 3006, p. 176, 1997
7. Q. Kim, T. J. Cunningham, and B. Pain, Characteristics of Monolithically Integrated InGaAs Active Pixel Image Array, SPIE Vol.3631, P. 122, 1999
8. Q. Kim, T. J. Cunningham, and B. Pain, Readout Characteristics of Integrated Monolithic InGaAs Active Pixel Sensor Array, SPIE Vol.3290, P. 278, 1998

9. P. Mouroulis, D. Wilson, P. D. Maker, and R. E. Muller, "Convex grating types for concentric imaging spectrometers," *Appl. Opt.* 37, 7200-7208 (1998).
10. P. Mouroulis: "Low-distortion imaging spectrometer designs utilizing convex gratings," in *International Optical Design Conference 1998*, SPIE Proc. 3482, 594-601 (1998).
11. P. Mouroulis and M. McKerns: "Pushbroom imaging spectrometer with high spectroscopic data fidelity: experimental demonstration", *Opt. Eng.* 39, 808-816 (2000)
12. P. Mouroulis, R. O. Green, and T. G. Chrien: "Design of pushbroom imaging spectrometers for optimum recovery of spectroscopic and spatial information," *Appl. Opt.* 39, 2210-2220 (2000).
13. P. D. Maker and R. E. Muller, "Phase holograms in polymethyl methacrylate", *J. Vac. Sci. Technol.* 10, 2516-2519 (1992).
14. P. D. Maker and R. E. Muller, "Continuous phase and amplitude holographic elements," U.S. pat. 5,393,634 (1995).
15. P. D. Maker, D. W. Wilson, and R. E. Muller, "Fabrication and performance of optical interconnect analog phase holograms made by E-beam lithography," in *Optoelectronic Interconnects and Packaging*, R. T. Chen and P. S. Guilfoyle Eds., vol. 62 of SPIE Critical Reviews Series, pp. 415-430 (1996).
16. John F. Mustard, Jessica M. Sunshine, C. M. Peters, A. Hoppin, and S. F. Pratt: "From minerals to rock: Toward modeling lithologies with remote Sensing, 24th Lunar and Planetary Science. Conference, Part 2: G-Mp.1041 (N94-16173 03-91).
17. Q. Kim and E. R. Fossum, "Wafer level damage assessment by test structures," *JPL D-12275*, 1995
18. S. K. Mendis, S. E. Kemeny, R. C. Gee, B. Pain, C. O. Staller, Q. Kim, and E. R. Fossum, "CMOS Active Pixel Image Sensors for Highly Integrated Image Systems," *IEEE J. of Solid-State Circuits*, Vol. 32, No. 2, p. 187 (1997)
19. T. Irifune, and A. E. Ringwood, "Phase Transformations in primitive MORB and pyrolite compositions to 25 GPa and some geophysical implications in *High Pressure Research in Mineral Physics*, Geophys. Monogr. Ser. Vol. 39, edited by M. Manghanani, and Y. Syono, pp. 231-242, 1987.
20. C. R. Bina and B. J. Wood, "Olivine-spinel transitions: Experimental and thermodynamic constraints and implications for the nature of the 400 km seismic discontinuity," *J. Geophys. Res.*, 92, 4853-4866, 1987.
21. H. St. C. O'Neill, D. C. Rubie, D. Canil, C. A. Geiger, C. R. Ross II, F. Seifert and A. B. Woodland, "Ferric iron in the upper mantle and in transition zone assemblages: Implications for relative oxygen fugacities in the mantle," in *Evolution of the Earth and Planets, Geophysics. Monogr. Ser. Vol. 74* edited by E. Takahashi, R. Jeanloz, and D. Rubie, pp. 73-88, 1993.
22. C. Maxwell, A. J. Volpe, C. W. Barlow, and W. S. Caughey, *Boch. Biophys. Res. Commun.*, 58, 166, 1974.
23. J. P. Collman, *Acc Chem. Res.*, 10, 625, 1977.
24. L. Vaska, *Acc. Chem. Res.*, 9, 175, 1970.
25. C. H. Barlow, J. C. Maxwell, W. J. Wallacw, and W. S. Caughey, *Biochem. Biophys. Res. Commun.*, 55, 91, 1974.
26. J. P. Collman, J. I. Brauman, T. R. Halburt, and K. S. Suslick, *Proc. Natl. Acad. Sci. USA*, 73, 3333, 1976.
27. J. M. Burke, J. R. Kincaid, S. Peters, R. R. Gagne, J. P. Collman, and T. G. Spiro, *J. Am. Chem. Soc.*, 100, 6083, 1978.
28. K. S. Suslick, Ph.D. Dissertation, Stanford University, 1978.
29. J. C. Maxwell and W. S. Caughey, *Biochem. Biophys. Res. Commun.*, 960, 1309, 1974.
30. J. D. Landels and G. A. Rodley, *Synth. Inorg. Met-Org. Chem.*, 2, 65, 1972.
31. D. A. White, A. J. Solodar, and M. M. Baizer, *Inorg. Chem.*, 11, 2160, 1972.